RESEARCH ARTICLE | DECEMBER 23 2025

From front-side to back-side illumination of InGaAs/InP SPADs for photon detection efficiency enhancement

Special Collection: Single-photon detectors: new physical principles, circuits and applications

S. Sorrentino; F. Telesca; D. Orlandelli; L. Finazzi; A. Tosi

APL Photonics 10, 120803 (2025)
https://doi.org/10.1063/5.0299841

APL Photonics ARTICLE pubs.aip.org/aip/app

From front-side to back-side illumination of InGaAs/InP SPADs for photon detection efficiency enhancement

Cite as: APL Photon. 10, 120803 (2025); doi: 10.1063/5.0299841
Submitted: 29 August 2025 • Accepted: 10 December 2025 •
Published Online: 23 December 2025

S. Sorrentino,[a)] F. Telesca, D. Orlandelli, L. Finazzi, and A. Tosi

AFFILIATIONS

Dipartimento di Elettronica Informazione e Bioingegneria, Politecnico di Milano, Milan 20133, Italy

Note: This paper is part of the Special Topic on Single-Photon Detectors: New Physical Principles, Circuits and Applications.
[a)]**Author to whom correspondence should be addressed:** simona.sorrentino@polimi.it

ABSTRACT

Low-noise front-side illuminated InGaAs/InP single photon avalanche diodes (SPADs) were converted into back-side illuminated ones to improve their photon detection efficiency (PDE). We introduced a mirror on the frontside and an antireflection-coated aperture on the backside, thus allowing photons to double-pass through the absorption InGaAs region. Such modifications did not affect the layer structure of the device and, consequently, its noise, while exploiting the double passage of photons to achieve higher PDE. In this work, we provide a direct comparison between the two structures, front-side illuminated (FSI) and back-side illuminated (BSI) SPADs, in terms of photon detection efficiency and dark count rate (DCR). Experimental results on devices with 10 μm and 25 μm active area diameters showcased a 24% increase in PDE, reaching up to 31% at 1550 nm and 5 V of excess bias, while maintaining the low DCR (a few kcps at 230 K) of the original FSI device.

I. INTRODUCTION

Single-Photon Avalanche Diodes (SPADs)[1] have become a convenient and widely used solution for detecting single photons up to 1.7 μm in various applications. They are compact, cost-effective, highly reliable, and easy to integrate into existing systems. These advantages, along with their ability to operate at temperatures accessible with thermoelectric coolers, make InGaAs-based SPADs ideal for SWIR (short-wave infrared) applications, such as LiDAR,[2] deep-space optical communication,[3] and near-infrared spectroscopy.[4] Furthermore, the growing interest in single-photon detectors is largely fueled by advances in quantum technology, where fields such as quantum communication,[5] quantum computing,[6] and quantum metrology[7] in the last years have required progressively more and more scalability, making the implementation of InGaAs/InP SPADs as the single photon detector of choice a cost-effective and practical solution. As these fields continue to evolve, improving the performance of InGaAs/InP SPADs also means balancing high photon detection efficiency (PDE) with minimal noise. For this purpose, back-side illumination (BSI) has gained attention in the literature as an effective solution to enhance PDE by using the same device layer stack—and, therefore, the same noise—while improving detection efficiency.

BSI configurations are widely used for silicon SPADs, particularly because they help increase the fill factor in arrays and, at the same time, the photon absorption probability in the near-infrared (NIR) range (thanks to thicker absorption regions and photon scattering structures).[8,9] For this reason, BSI SPAD structures—often combined with 3D stacking technology and microlenses—are extensively investigated and optimized to improve efficiency, especially at longer wavelengths (for LiDAR applications).[10] In detail, when BSI structures are derived from FSI ones with similar base designs, the PDE is strongly enhanced (e.g., a factor 2 in Ref. 11), thanks to reflective and diffusive structures that lead to multiple passages of the photons through the active region. However, in silicon detectors we must consider that, when flipping the photodetector for BSI, the remaining silicon substrate thickness plays a key role in defining the PDE:[12] a thick substrate will reduce the PDE, especially at short wavelengths, while an optimal thin substrate requires advanced thinning procedures. BSI InGaAs/InP SPADs have been developed by different research groups and companies, and their PDE is superior to the FSI counterparts[13–16] In this work, we aim to investigate the contributions to the PDE from the different structures present in FSI and BSI InGaAs/InP SPADs, where materials and wavelengths are different from the silicon detector case. We aimed to add a comparative analysis between FSI and BSI, with a simple, repeatable, and cost-effective processing approach that can be performed on already fabricated and diced detectors (few square millimeters area), without the need of dedicated expensive production runs.

To this aim, we propose a comparison between well-performing FSI SPAD devices (published by Signorelli *et al.*[1]) and structurally identical devices that were reprocessed to operate in a back-side illuminated configuration. The approach we used is expected to improve the trade-off between PDE and DCR (Dark Count Rate) by exploiting double pass of incoming photons, effectively increasing the equivalent absorption layer thickness without modifying the total volume, thus not worsening its DCR.

As depicted in Fig. 1 and better discussed in Sec. II, in a FSI configuration, photons that are not initially absorbed in the InGaAs layer must propagate through over 100 μm of InP substrate before reaching a reflective interface, in particular, the 200-nm-thick titanium layer located at the cathode, which exhibits poor reflectivity. Even when reflection occurs, the long distance between the InP–cathode interface and the absorption layer causes photons that are backscattered at small angles to re-enter the InGaAs layer outside the active region, thus not triggering avalanches. On the other hand, in a BSI configuration, photons entering from the backside and not being absorbed by the InGaAs layer are reflected at the interface with the aluminum layer on the frontside, which is just about 3 μm from the absorption layer, ultimately increasing their probability of being absorbed in the active region even when traveling with small angles. To quantify the improvement of the device performance when switching from one configuration to the other, in this paper, we propose a direct comparison between structures with identical internal layers and from the same wafer.

II. DEVICE STRUCTURE

The devices described here are based on the typical separate absorption, grading, charge, and multiplication (SAGCM) heterostructure of InGaAs/InP SPADs, as shown in Fig. 1, with a double p^+-zinc diffusion to define the active area of the detector. In the front-illuminated planar configuration [Fig. 1(a)], a single photon, with a wavelength of up to about 1.7 μm, enters the structure from the top aperture of the device and can be absorbed in the InGaAs layer. The photogenerated hole is then drifted toward the

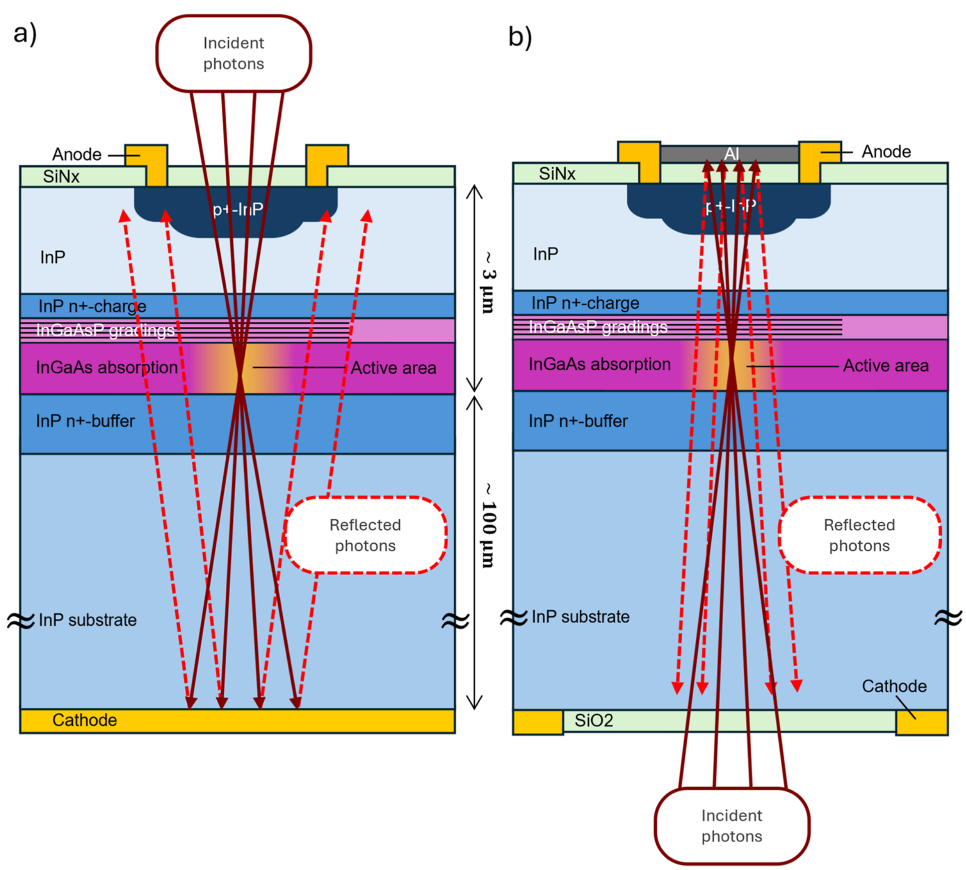

FIG. 1. Comparison between FSI and BSI InGaAs/InP SPADs. In the FSI SPAD, (a) photons can enter the device from the aperture on the front-side of the chip and reach the InGaAs absorption region, while in the BSI SPAD, (b) photons entering from the back-side can cross the active area twice when reflected from the Al layer at the front. Please note that the drawing is not to scale, as a substrate thicker than 100 μm is only partially depicted.

InP cap region, facilitated by quaternary InGaAsP grading layers.[17] In the layer between the double-zinc diffusion and the charge layer, the electric field is strong enough to initiate a self-sustaining avalanche with high probability through the impact ionization process,[18] and the resulting macroscopic current signal can then be easily read by an external circuit.

The thickness of the InGaAs absorption layer is a key factor in SPAD operation, as it simultaneously impacts photon detection efficiency, dark count rate, and timing jitter. A thicker absorption layer captures more photons, thereby improving the PDE. However, a larger active volume introduces more defects, and this results in an increase in DCR. In addition, enlarging the thickness of such layer would also introduce a greater variation in the hole transit time across the absorption layer, worsening the timing jitter of the device. Therefore, the optimal solution would be to keep the InGaAs layer thin for low noise and low timing jitter, but at the same time to modify the structure to achieve higher PDE.

To this end, the previously fabricated front-side illuminated SPADs with thin (1 μm) InGaAs layer were further processed at Polifab,[19] the cleanroom facility of Politecnico di Milano, with modifications applied to both the front and back sides of the devices.

Front-side processing aimed to close the top entrance aperture by thermally evaporating an 80-nm-thick aluminum layer. Such layer is located at a very short distance from the active area, meaning that a non-negligible fraction of photons arriving from the backside, which are not absorbed during the first pass, will re-cross the active area.

In front-side illuminated devices, a portion of the unabsorbed photons entering through the top aperture is also reflected back at the cathode interface, but such contribution might be significantly small. Ohmic contacts in the devices under test are constituted by a layer stack of Ti/Pt/Au: gold is a high electrical conductivity material, ensuring high reflectivity at its interface and thus reducing the optical loss; however, a pure gold contact has very poor adhesion and therefore requires the addition of a thinner layer of titanium to improve surface adhesion, together with a thin platinum layer in between as a diffusion barrier.[20,21] For this reason, the interface at the cathode at the bottom part of the device is constituted by a thick layer of InP (more than 100 μm) and a 200-nm-thick Ti layer. Given titanium's optical constants,[22,23] the calculated reflectivity at such interface is around 30% for photons at 1550 nm, with a high percentage of photons being absorbed in the Ti layer. Such a percentage would result in a small yet measurable contribution to the overall PDE of the device. Therefore, it would be possible to quantify the reflections at the cathode by comparing efficiency measurements between SPADs with and without the cathode.

Nevertheless, we have to consider that photons entering from the top aperture have slightly different propagation directions, given by the numerical aperture of the lens used in our optical system. This implies that peripheral photons impinging even with a small angle with respect to the normal to the InP/Ti interface, when reflected, would most likely cross the InGaAs layer outside the active area, due to the large distance that separates the reflective cathode contact and the InGaAs layer. As a result, they do not contribute to the PDE. To support this point and evaluate the contribution of reflections from the cathode, both simulations and measurements were carried out on FSI SPADs. First, we performed ray-tracing simulations (with Zemax[24]) of our optical system, which consists of a single-mode fiber (SMF28), a collimator (output beam diameter = 3.6 mm, NA = 0.15, f = 18.75 mm), and a focusing lens (NA = 0.25, f = 11.3 mm), along with the SPAD layer stack positioned at a distance of 11.3 mm from the lens. To simplify the simulation, we considered only the effect of the aspheric lens focusing a perfectly collimated light beam onto the SPAD. By simulating the entrance of an optical beam into the device, the irradiance of the beam can be evaluated along a plane within the absorption layer (see the A–A′ plane in Fig. 2), both with and without reflections from the cathode. Figure 3 shows the simulated irradiance along the device cross-section (with X = 0 corresponding to the center of the active area) for two cases: a non-reflective cathode (red curve) and a perfectly reflective cathode that reflects 100% of the incident light (black curve). Results reveal that the central irradiance peak overlaps in the two cases and, considering the integral over the active area, only a negligible increase of 0.87% in total irradiance is registered when cathode reflections are included in the simulation. This demonstrates that no significant portion of the beam re-enters the InGaAs layer in the active region, even with 100% reflectivity. In addition, we fabricated FSI SPADs without the cathode contact under the SPAD active area: we dry-etched the cathode metal layer in correspondence of the active area, and then, we illuminated the structures from the

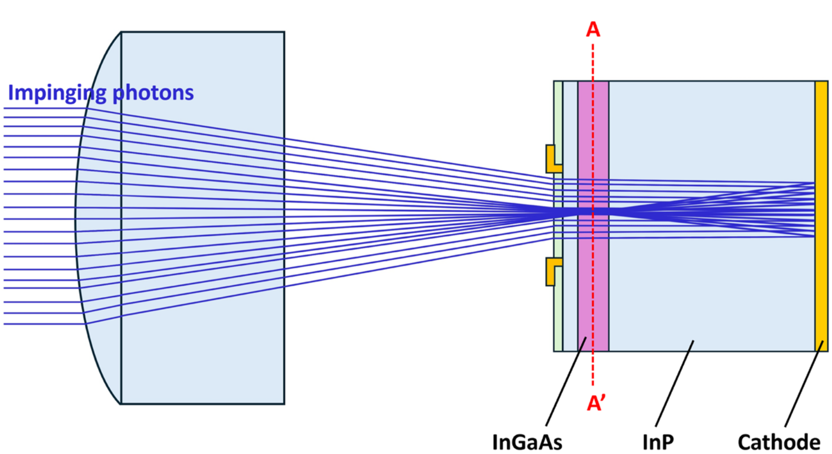

FIG. 2. Schematic representation of the optical system and the SPAD, not to scale. Impinging photons are focused by the optical system inside the absorption layer; then, a portion of photons not absorbed during the first passage is reflected at the cathode.

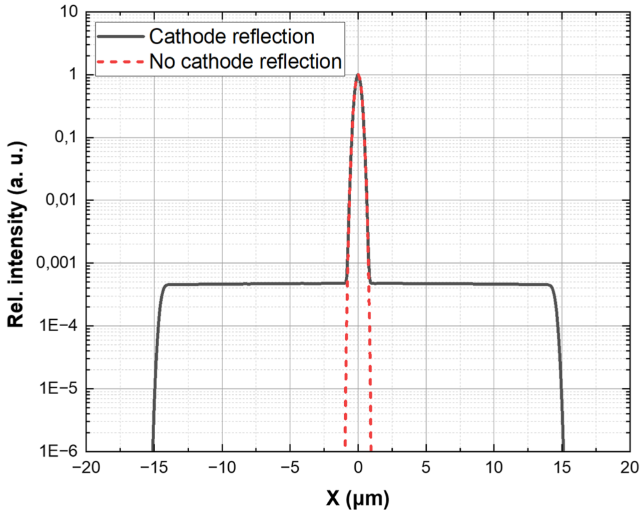

FIG. 3. Relative intensity of the irradiance cut along the A–A′ plane, represented by the red dashed line in Fig. 2. X = 0 corresponds to the center of the device.

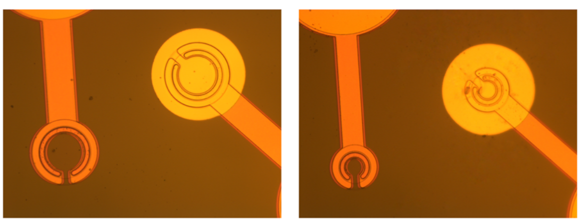

FIG. 4. Microscope images of 25 μm (left) and 10 μm active-area (right) SPADs, with and without Al. The Al layer deposited onto the devices on the right is measured to be 80 nm thick.

front side. This allowed us to compare two samples that are identical in terms of illumination direction, layer stack, and front-side anti-reflection coating, with the only difference being the presence or absence of the cathode metal contact and thus the expected reflection contribution. Such measurements are reported and commented in Sec. III, among the experimental results, and proved that there is no contribution to the PDE from the reflection at the cathode.

As a result of the investigation described above, placing a reflective layer in close proximity to the active area plays a crucial role in ensuring that a high fraction of photons is reflected back into the active region. Consequently, the double-pass event in the BSI configuration is expected to involve a significantly larger fraction of photons compared to the FSI case, leading to a notable impact on the PDE of the device.

To investigate performance enhancement through a simple, repeatable, and cost-effective approach, we chose aluminum to create a simple metallic layer as a top reflector. 80 nm of Al were deposited on top of the SiN layer present on the front of the device, providing between 93% and 98% of reflectivity depending on the optical constants considered.[25,26] The main advantage of Al over other highly reflective materials, such as Ag or Au, lies in its excellent adhesion when deposited on SiN. In contrast, these other metals typically require an intermediate adhesion layer, usually made of Ti or Cr—materials that are known to absorb light at 1550 nm. Although the thickness of such adhesion layers is generally very small (5 nm or less), the absorption introduced goes up to more than 30%. For this reason, Al constitutes a more advantageous choice overall.

Figure 4 shows microscope pictures of 25-μm and 10-μm active-area SPADs without (left) and with (right) the Al layer over the active area. Step height measurements performed with a surface profiler on the two adjacent 25 μm active-area devices confirm an Al layer thickness of 80 nm, as shown in Fig. 5.

Subsequently, processing on the back-side of the device was required in order to create an entrance aperture for photons. Ion beam etching was employed to pattern the cathode metal contact. Figure 6 reports a profiler measurement performed on the back of the device showing the step between the original cathode metal contact and the exposed InP substrate. Indeed, around the back entrance, the metallic Ti/Pt/Au stack was left in order to preserve the electrical cathode contact of the device. As visible from the steep change in scanned height in Fig. 6, the chip height is reduced by 1.2 μm, meaning that all of the metallic cathode contact (having a total thickness of 1 μm) has been removed, together with 200 nm of InP from the substrate.

Finally, to maximize light transmission to the InP substrate, 270 nm of SiO_2 were deposited by sputtering, providing an antireflection coating with transmittance of 96% at 1550 nm. After the above-mentioned steps, the final device structure is the one depicted in Fig. 1(b).

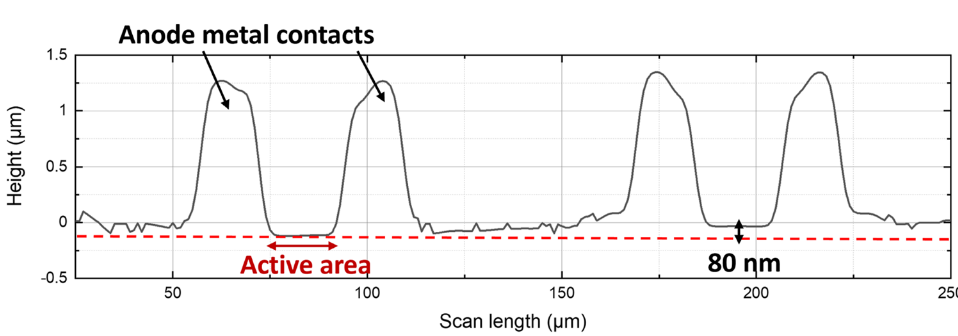

FIG. 5. Profiler images of the front side obtained by scanning two adjacent 25 μm active-area SPADs laying on the same chip: the first one without Al (on the left), the second with Al deposited on the active area (on the right). The height difference between the two cases is ∼80 nm, corresponding to the thickness of the deposited Al layer. The scanning vertical resolution is 1.7 Å, while the horizontal resolution is limited to 2 μm by the stylus tip radius.

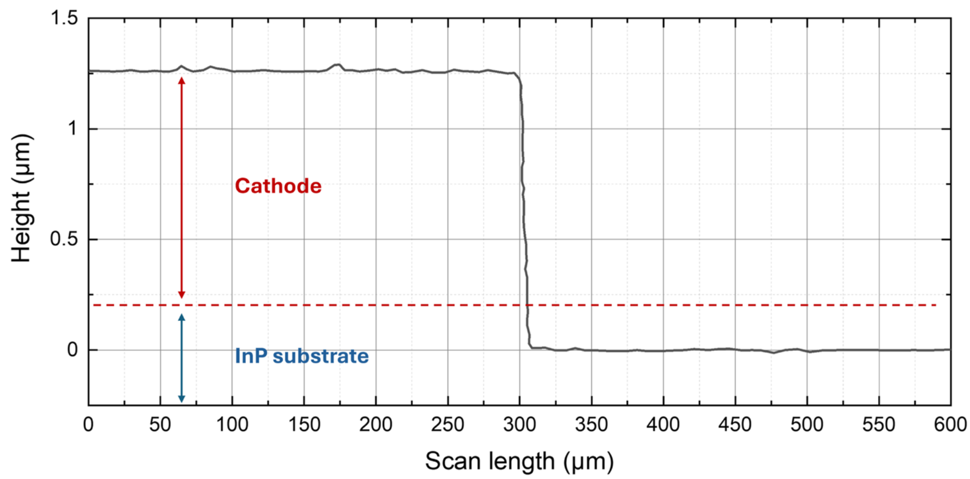

FIG. 6. Profiler images of the backside obtained by scanning a large area of the chip. The scanned region corresponds to the transition zone from the area with the cathode to the area where the cathode has been removed, revealing a step exceeding 1 μm in height. The scanning vertical resolution is 1.7 Å, while the horizontal resolution is limited to 2 μm by the stylus tip radius.

III. EXPERIMENTAL RESULTS

The measurements of four BSI SPADs were carried out by operating the detectors in gated mode, using an ON-time of T_{ON} = 100 ns. During the OFF-time, the SPAD is biased 0.5 V below its breakdown voltage. During the ON-time, an excess bias voltage (V_{EX}) of 5 V is applied above the breakdown voltage. A 1 kΩ resistor is used in series with the SPAD to reduce the avalanche current, although full quenching is reached only when the SPAD voltage is lowered below breakdown at the end of the gate ON-time.

A. I–V curve

Figure 7 shows the current–voltage (I–V) characteristics of two 10 μm active-area SPADs, with front-side and back-side illumination, at a temperature of 230 K. The breakdown voltage is about 66 V. The sharp and steep rise indicates that most of the active region undergoes breakdown at this voltage, with minimal influence from edge effects. The punch-through voltage, i.e., the reverse bias at which the InGaAs absorption layer is depleted, is at about 50 V, as clearly visible in the photocurrent curves, obtained upon illuminating the SPADs.

The comparison between the I–V curves of the two cases confirms that both the breakdown and the punch-through voltages did not change during the conversion from FSI to BSI.

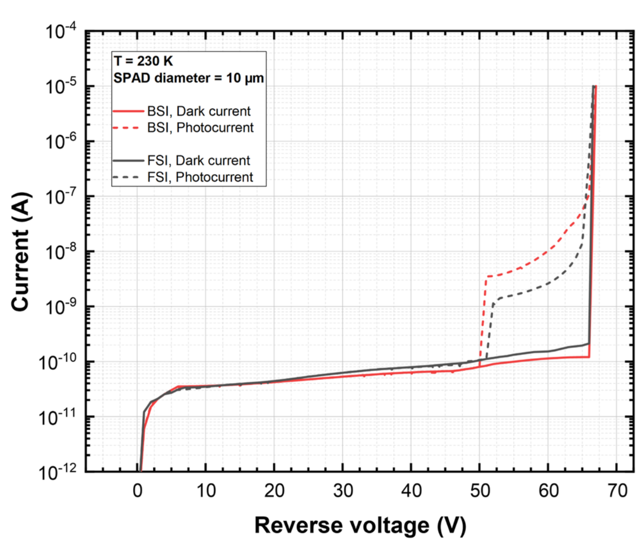

FIG. 7. Current–voltage curves of BSI and FSI devices at 230 K. Each device was tested both in dark conditions and upon illumination.

B. Dark count rate

We measured the primary dark count rate (DCR) of the SPADs, which arises from thermal and field-assisted carrier generation, at various excess bias voltages.

Figure 8 shows the DCR measurements performed on SPADs with 25 μm active area diameter, at 5 V of excess bias and with various OFF-times. The same plot reports measurements of both back-side illuminated devices and front-side illuminated ones: the overall dependence of DCR on the OFF time is the same for both cases, with low count rate at long OFF-times and a steep increase at short OFF times, caused by afterpulsing phenomena introduced by trapped carriers.[1]

Both BSI and FSI devices show a DCR of few kcps at, respectively, 230 and 225 K (at 100 μs OFF-time and 5 V of excess bias DCR is on average ~9700 cps). Similar results were obtained when measuring the 10 μm active-area SPADs (Fig. 9), showing lower dark count rates, as expected, due to their reduced active volume. Indeed, with a 100 μs OFF-time, the DCR at 230 K is ~2900 cps for BSI SPADs, and ~6400 cps for FSI ones at 225 K. The difference in DCR is within the statistical variation between devices from the same wafer.

Such measurements assess that no additional noise was introduced during the lithographic, deposition, and etching phases of the FSI-to-BSI conversion process.

C. Photon detection efficiency

We measured the photon detection efficiency of the 10 μm and 25 μm active-area devices by means of a continuous wave laser at a

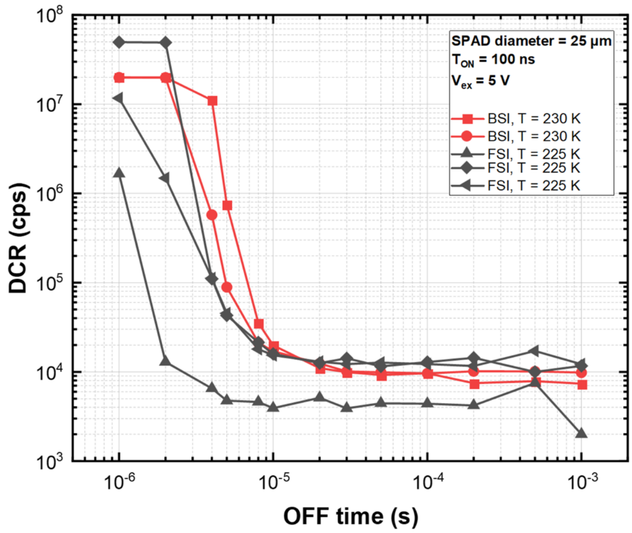

FIG. 8. DCR as a function of the square wave gate period for BSI devices compared to FSI ones, at 5 V excess bias voltage. The gate ON time (T_{ON}) is set to 100 ns. The active area diameter of these detectors is 25 μm.

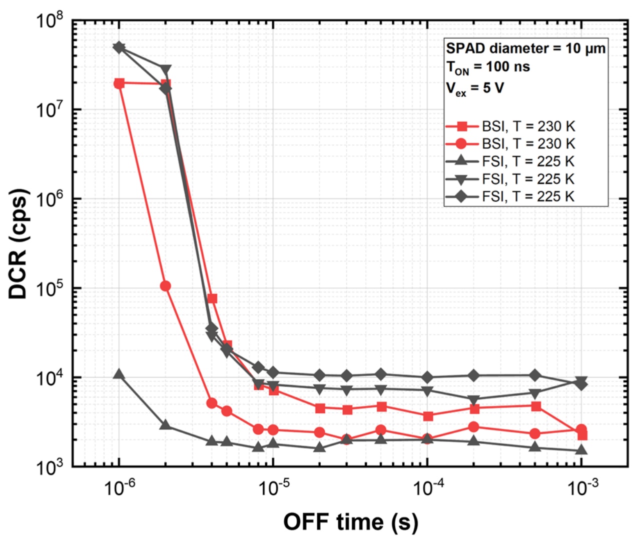

FIG. 9. DCR as a function of the square wave gate period for BSI devices compared to FSI ones, at 5 V excess bias voltage. The gate ON time (T_{ON}) is set to 100 ns. The active area diameter of these detectors is 10 μm.

wavelength of 1550 nm, focused onto the active area of the SPADs with the same optical system described in Sec. II. The laser beam is split into two channels: 99% of the power is sent to a powermeter, while the remaining 1% is directed onto the SPAD. The system is calibrated using a photodiode and then the 1% channel is further attenuated to reach the single-photon regime. During the measurements, the optical power is continuously monitored through the powermeter to accurately determine the real-time power incident on the SPAD, enabling a precise evaluation of the device efficiency. In

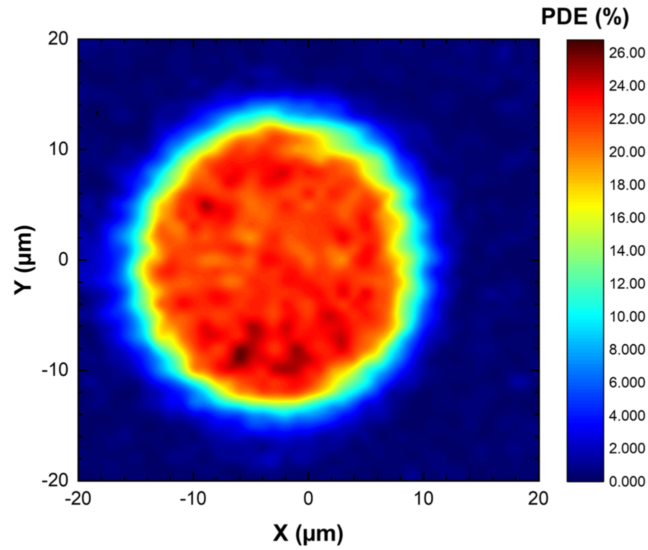

FIG. 10. PDE map of the 25 μm active-area SPAD without the cathode contact, when front-side illuminated. Measurements were performed at 5 V of excess bias voltage, scanning the active area with a continuous-wave 1550 nm laser. The light spot is about 6 μm in diameter.

order to operate in single-photon regime with no pile-up distortion, the count rate was kept below 5% of the gate rate.[27] The 2D PDE maps were acquired scanning the active area of the devices with a 6 μm spot size laser and a step size of 1 μm.

First, we measured the photon detection efficiency of the SPADs without the cathode, to confirm that reflections occurring at the cathode do not contribute to the final efficiency of the device. The SPAD is illuminated from the frontside; therefore, the two SPADs under test, with and without the cathode, were measured under identical experimental conditions, while sharing the same layer stack and anti-reflection coating. This ensures that any changes in efficiency can be attributed exclusively to the contribution of the cathode reflectance. The results are shown in Fig. 10, where it can be observed that the average efficiency falls within the statistical range of previously tested FSI SPADs with the cathode metal contact,[1] with an average PDE between 24% and 25%, and peaks around 26%. Such study definitively establishes that the observed PDE is exclusively determined by the first passage of photons through the active area of the device.

Subsequently, we proceeded to investigate the BSI structures. It is known that the PDE of a SPAD detector is given by two contributions: the probability that a photon crossing the active area is absorbed (i.e., the absorption efficiency) and the probability that the photogenerated carriers ignite an avalanche (i.e., the avalanche triggering probability). When converting a front-side illuminated structure into a back-side illuminated one, the latter contribution remains unaltered, since it is related to the electric field inside the device, in turn regulated by the multiplication layer thickness and by the doping and shaping of the double zinc diffusion. However, exploiting the double passage of photons through the active area results in a higher absorption efficiency, giving an overall higher expected PDE.

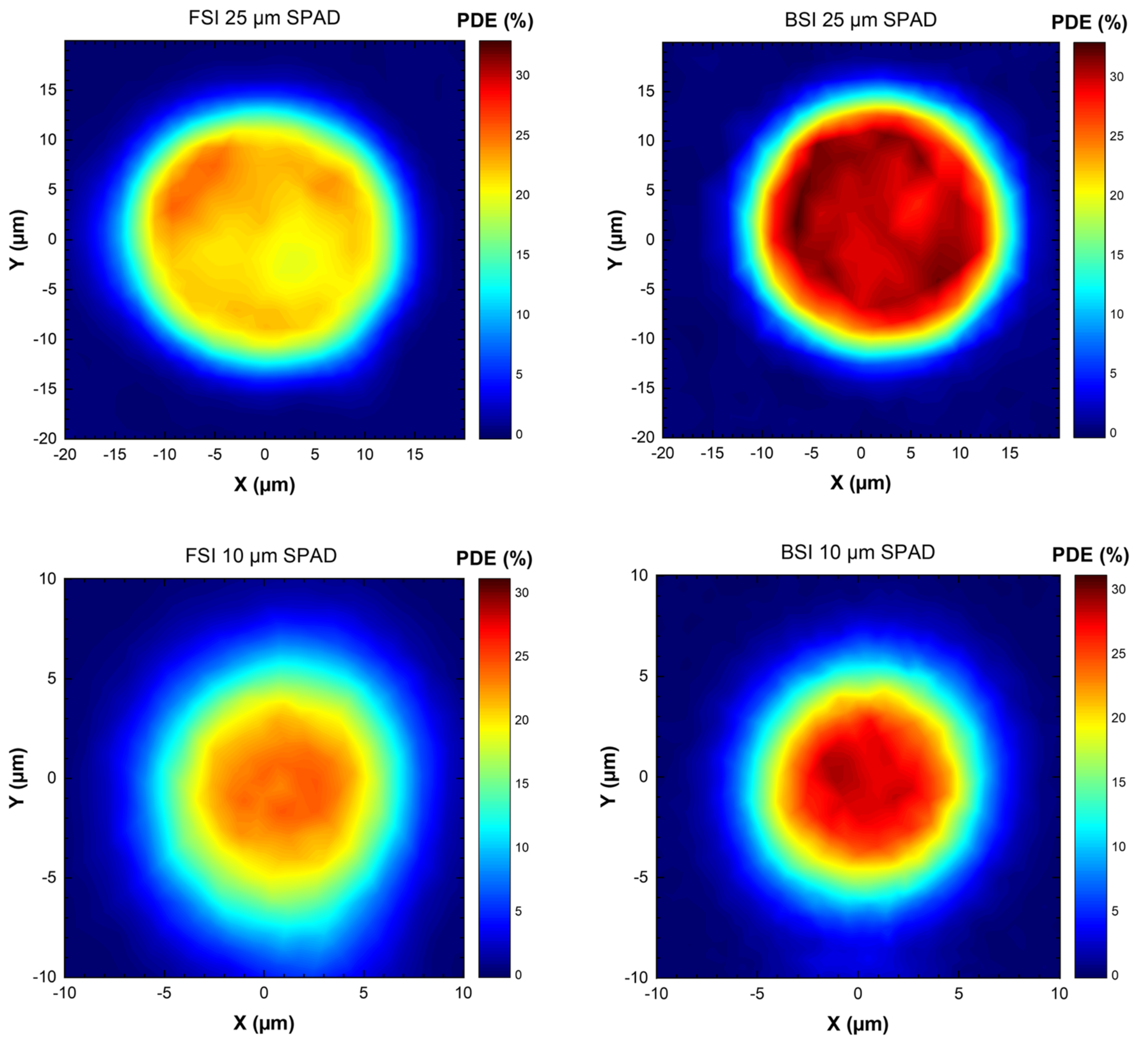

FIG. 11. PDE maps of the 25 μm (top) and 10 μm (bottom) active-area SPADs, with front-side (left) and back-side (right) illumination. Measurements were performed at 5 V of excess bias voltage, scanning the active area with a 1550 nm continuous-wave laser. The light spot is about 6 μm in diameter.

Measurements of the 25 μm active-area SPADs are shown in Fig. 11 for the front-side illuminated device and for the back-side illuminated one. As already published,[1] our FSI SPADs achieve efficiency peaks around 26% at 1550 nm with an excess bias voltage of 5 V. In the same conditions, PDE peaks for back-side illuminated devices are found beyond 31%. Both FSI and BSI SPADs show non-uniformities in the PDE maps (as reported in Ref. 1), due to higher electric field at the edge (as expected from device design), non-uniform Zn diffusion depth, and interference phenomena introduced by back-end-of-line structures. In addition, in BSI devices, the rear aperture results from dry-etching and antireflection coating deposition by sputtering, possibly leading to slightly rough surface. A direct comparison between the two cases is provided in Fig. 12, where the PDE is plotted as a function of the X direction, performing a horizontal cut along Y = 0 μm.

Similarly, PDE measurements of the 10 μm active-area SPADs are reported in Fig. 11 for the two configurations. From the comparison of the PDE values in the two cases (see Fig. 13), we can appreciate a photon detection efficiency increase from 25% to 31% when switching to a back-side illumination, providing a 24% PDE enhancement.

To estimate the maximum expected PDE, we performed ray-tracing simulations (similar to the Zemax-based ones described in Sec. II) for both FSI and BSI configurations. Assuming a perfectly reflective metal layer, the expected PDE enhancement is about 33% when switching from FSI to BSI. The difference between experimental results and simulations can be attributed to several factors, such as the actual Al reflectivity (93%–98%), imperfections at the back entrance surface caused by dry-etching and sputtering of the anti-reflection coating, and structural non-uniformities in the SPADs

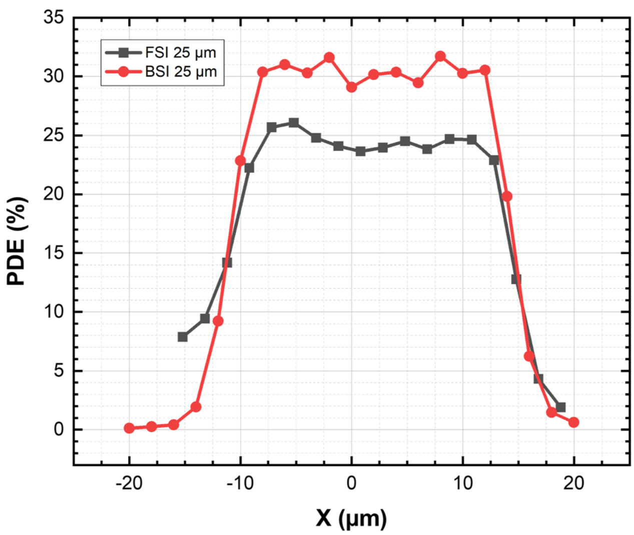

FIG. 12. Comparison of the PDE values for the 25 μm active-area SPADs, with front-side and back-side illumination, at 5 V of excess bias voltage. The plot is obtained extracting the PDE data at Y = 0 μm from the PDE maps.

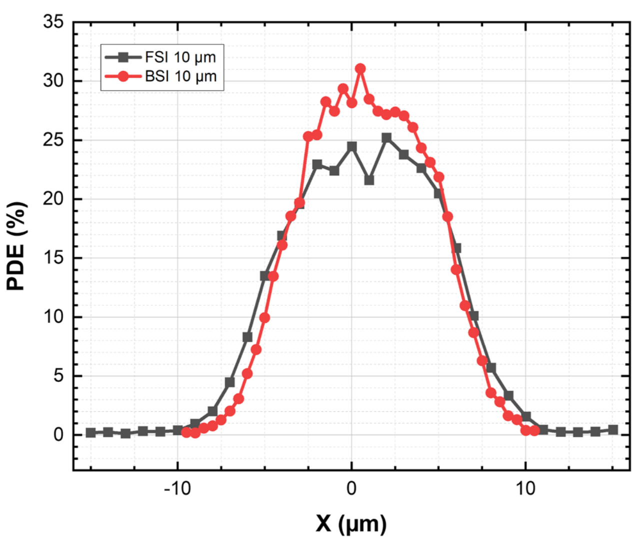

FIG. 13. Comparison of the PDE values for the 10 μm active-area SPADs, with front-side and back-side illumination, at 5 V of excess bias voltage. The plot is obtained extracting the PDE data at Y = 0 μm from the PDE maps.

related to the zinc diffusion profile and the resulting non-uniform avalanche triggering probability.

IV. CONCLUSIONS

In this work, we proposed a quantitative performance comparison between FSI and BSI SPAD structures by considering devices fabricated on the same wafer, and therefore sharing the same layer stack and design, with the only difference being the FSI or BSI configuration. We investigated how the noise and efficiency performance of the state-of-the-art FSI InGaAs/InP SPADs are affected by the FSI-to-BSI conversion, consisting of depositing a highly reflective layer on the front side and creating a photon entrance on the back side. We then compared the performance of the converted devices to their unmodified counterparts.

We quantified the resulting efficiency enhancement and demonstrated that a consistent increase in photon detection efficiency (PDE), up to 24%, can be achieved only by introducing a few additional processing steps, thus maintaining the same layer structure, internal electric fields, and primary dark count rate (DCR). The resulting devices exhibit PDE values of 31% and dark counts in the few-kcps range at 230 K and 5 V excess bias.

Moreover, the contribution to the total PDE given by reflections from the cathode contact is better clarified in a front-side illuminated configuration, assessing that the 25% PDE must be attributed solely to the first passage of photons through the active area, while the small percentage of light reflected at the cathode does not impact the total efficiency when considering the full experimental optical setup.

The here-presented results constitute a practical, scalable, and easy-to-implement strategy for enhancing SPAD performance, especially in applications requiring both high efficiency and low noise, such as quantum communication, quantum computing, and quantum metrology.

ACKNOWLEDGMENTS

This work was supported by the European Union's Horizon Europe Research and Innovation Program under Project No. QPIC1550, Grant Agreement No 101135785. Views and opinions expressed are, however, those of the authors only and do not necessarily reflect those of the European Union. Neither the European Union nor the granting authority can be held responsible for them.

AUTHOR DECLARATIONS

Conflict of Interest

The authors have no conflicts to disclose.

Author Contributions

S.S., F.T., and A.T. contributed to conceptualization. S.S. was responsible for data curation, investigation, and validation, under the supervision of F.T. and A.T.. D.O. supported data curation and, together with L.F., contributed to the software aspects. Writing was carried out by S.S., under the supervision of A.T.

S. Sorrentino: Conceptualization (equal); Data curation (equal); Software (equal); Writing – review & editing (equal). **F. Telesca**: Conceptualization (equal); Supervision (equal). **D. Orlandelli**: Data curation (supporting); Software (equal). **L. Finazzi**: Software (supporting). **A. Tosi**: Conceptualization (equal); Supervision (equal); Writing – review & editing (equal).

DATA AVAILABILITY

The data that support the findings of this study are available from the corresponding author upon reasonable request.

REFERENCES

[1] F. Signorelli, F. Telesca, E. Conca, A. D. Frera, A. Ruggeri, A. Giudice, and A. Tosi, "Low-noise InGaAs/InP single-photon avalanche diodes for fiber-based and free-space applications," IEEE J. Sel. Top. Quantum Electron. **28**, 3801310 (2022).

[2] C. Yu, M. Shangguan, H. Xia, J. Zhang, X. Dou, and J.-W. Pan, "Fully integrated free-running InGaAs/InP single-photon detector for accurate lidar applications," Opt. Express **25**, 14611–14620 (2017).

[3] A. Biswas, M. Srinivasan, K. Andrews, A. Velasco, E. Alerstam, J. Allmaras, E. Wollman, S. Meenehan, M. Wright, and R. Rogalin, "Overview of the deep space optical communications (DSOC) technology demonstration," Proc. SPIE **13355**, 133550J (2025).

[4] S. A. Carp, D. Tamborini, D. Mazumder, K.-C. Wu, M. R. Robinson, K. A. Stephens, O. Shatrovoy, N. Lue, N. Ozana, M. H. Blackwell *et al.*, "Diffuse correlation spectroscopy measurements of blood flow using 1064 nm light," J. Biomed. Opt. **25**, 097003 (2020).

[5] N. Gisin and R. Thew, "Quantum communication," Nat. Photonics **1**, 165–171 (2007).

[6] J. L. O'brien, "Optical quantum computing," Science **318**, 1567–1570 (2007).

[7] V. Giovannetti, S. Lloyd, and L. Maccone, "Advances in quantum metrology," Nat. Photonics **5**, 222–229 (2011).

[8] T. Al Abbas, N. Dutton, O. Almer, S. Pellegrini, Y. Henrion, and R. Henderson, "Backside illuminated SPAD image sensor with 7.83 μm pitch in 3D-stacked CMOS technology," in *2016 IEEE International Electron Devices Meeting (IEDM)* (IEEE, 2016), pp. 8–1.

[9] M. Wojtkiewicz, B. Rae, and R. K. Henderson, "Review of back-side illuminated 3-D-stacked SPADs for time-of-flight and single-photon imaging," IEEE Trans. Electron Devices **71**, 3470–3477 (2024).

[10] E. Park, W.-Y. Ha, H.-S. Park, D. Eom, H.-S. Choi, D.-H. Ahn, W.-Y. Choi, and M.-J. Lee, "A back-illuminated SPAD fabricated with 40 nm CMOS image sensor technology achieving near 40% PDP at 940 nm," IEEE J. Sel. Top. Quantum Electron. **30**, 3800207 (2024).

[11] E. Van Sieleghem, G. Karve, K. De Munck, A. Vinci, C. Cavaco, A. Süss, C. Van Hoof, and J. Lee, "A backside-illuminated charge-focusing silicon SPAD with enhanced near-infrared sensitivity," IEEE Trans. Electron Devices **69**, 1129–1136 (2022).

[12] B. Vereecke, C. Cavaco, K. De Munck, L. Haspeslagh, K. Minoglou, G. Moore, D. Sabuncuoglu, K. Tack, B. Wu, and H. Osman, "Quantum efficiency and dark current evaluation of a backside illuminated CMOS image sensor," Jpn. J. Appl. Phys. **54**, 04DE09 (2015).

[13] J. Zhang, M. A. Itzler, H. Zbinden, and J.-W. Pan, "Advances in InGaAs/InP single-photon detector systems for quantum communication," Light: Sci. Appl. **4**, e286 (2015).

[14] B. Zhang, S. Yin, Y. Liu, Z. Jiang, W. He, Q. Li, J. Hao, and L. Wang, "High performance InGaAs/InP single-photon avalanche diode using DBR-metal reflector and backside micro-lens," J. Lightwave Technol. **40**, 3832–3838 (2022).

[15] Y.-Q. Fang, W. Chen, T.-H. Ao, C. Liu, L. Wang, X.-J. Gao, J. Zhang, and J.-W. Pan, "InGaAs/InP single-photon detectors with 60% detection efficiency at 1550 nm," Rev. Sci. Instrum. **91**, 083102 (2020).

[16] S.-H. Baek, S.-C. Yang, C.-Y. Park, C.-W. Park, S.-B. Cho, and S.-W. Ryu, "Room temperature quantum key distribution characteristics of low-noise InGaAs/InP single-photon avalanche diode," J. Korean Phys. Soc. **78**, 634–641 (2021).

[17] J. C. Campbell, A. G. Dentai, W. S. Holden, and B. L. Kasper, "High-performance avalanche photodiode with separate absorption 'grading' and multiplication regions," Electron. Lett. **19**, 818–820 (1983).

[18] Y. Okuto and C. R. Crowell, "Energy-conservation considerations in the characterization of impact ionization in semiconductors," Phys. Rev. B **6**, 3076 (1972).

[19] Polifab, Politecnico di Milano, https://www.polifab.polimi.it/.

[20] G. M. Smith, D. V. Forbes, R. M. Lammert, and J. J. Coleman, "Metallization to asymmetric cladding separate confinement heterostructure lasers," Appl. Phys. Lett. **67**, 3847–3849 (1995).

[21] V. L. Rideout, "A review of the theory and technology for ohmic contacts to group III–V compound semiconductors," Solid-State Electron. **18**, 541–550 (1975).

[22] P. Johnson and R. Christy, "Optical constants of transition metals: Ti, V, Cr, Mn, Fe, Co, Ni, and Pd," Phys. Rev. B **9**, 5056 (1974).

[23] D. W. Lynch, C. G. Olson, and J. H. Weaver, "Optical properties of Ti, Zr, and Hf from 0.15 to 30 eV," Phys. Rev. B **11**, 3617 (1975).

[24] Ansys Zemax OpticStudio, https://www.ansys.com/products/optics/ansys-zemax-opticstudio.

[25] A. D. Rakić, "Algorithm for the determination of intrinsic optical constants of metal films: Application to aluminum," Appl. Opt. **34**, 4755–4767 (1995).

[26] H. E. Bennett, M. Silver, and E. J. Ashley, "Infrared reflectance of aluminum evaporated in ultra-high vacuum," J. Opt. Soc. Am. **53**, 1089–1095 (1963).

[27] D. O'Connor, *Time-Correlated Single Photon Counting* (Academic Press, 1984).